A&A 414, 1081–1090 (2004)
DOI: 10.1051/0004-6361:20034037

Astronomy & Astrophysics

Non-adiabatic theoretical observables in δ Scuti stars

A. Moya[1], R. Garrido[1], and M. A. Dupret[1,2,⋆]

[1] Instituto de Astrofísica de Andalucía-CSIC, Granada, Spain
[2] Institut d'Astrophysique et de Géophysique de l'Université de Liège, Belgium

Received 2 July 2003 / Accepted 28 October 2003

Abstract. Phase differences and amplitude ratios at different colour photometric bands are currently being used to discriminate pulsation modes to facilitate mode identification of κ-driven non-radial pulsating stars. In addition to physical inputs (e.g., mass, $T_{\rm eff}$, etc.), these quantities depend on the non-adiabatic treatment of the atmosphere. This paper presents theoretical results concerning δ Scuti pulsating stars. The envelope of each of these stellar structures possesses a convection zone whose development is determined by various factors. An interacting pulsation-atmosphere physical treatment is introduced which supplies two basic non-adiabatic physical quantities: the relative effective temperature variation and the phase lag $\phi^{\rm T}$, defined as the angle between effective temperature variation and radial displacement. These quantities can be used to derive the phase differences and amplitude ratios. Numerical values for these quantities depend critically on the α MLT parameter used to calculate the convection in the envelope. The dependence on α was analyzed and it was found that the use of colour observations may be of considerable importance in testing the MLT. Finally, examples are given of how α introduces uncertainties in the theoretical predictions regarding phases and amplitudes of photometric variations in δ Scuti pulsating stars.

Key words. stars: variables: δ Scuti – stars: atmosphere – stars: oscillations

1. Introduction

Asteroseismology is presently being developed as an efficient instrument in the study of stellar interiors and evolution. Pulsational periods are the most important asteroseismological observational inputs. However, for non-solar like oscillations, such as those characterizing δ Scuti stars, the information contained in these periods is not sufficient to adequately constrain theoretical predictions. Without additional observational data, mode identification is, therefore, not feasible in non-solar like contexts. The primary obstacles are that the pulsation modes of δ Scuti stars: 1) do not lie within the asymptotic regime and 2) may be affected by the "avoided crossing" phenomenon. Furthermore, rotation and eventual coupling also destroy any possible regular pattern.

One way to obtain more information on the basis of photometric observations is to study the multicolor flux variations. The linear approximation to non-radial flux variations of a pulsating star was first derived by Dziembowski (1977b), and later reformulated by Balona & Stobie (1979a, 1979b) and by Watson (1988). In Garrido et al. (1990), the linear approximation was successfully used to discriminate the spherical orders l of these pulsating star modes. Several attempts to fit observations have shown that the method can be applied, at least to low rotational velocities (e.g., FG Vir in Breger et al. 1999; BI CMi in Breger et al. 2002; 4 CVn in Breger et al. 1999; V1162 in Arentoft et al. 2001 and some other stars in Garrido 2000; for fast rotators, see Daszyńska et al. 2002).

Most theoretical and numerical pulsation models have been developed using the adiabatic approximation (Christensen-Dalsgaard 1982; Tran & Leon 1995). However, pulsation is highly non-adiabatic in stellar surface layers, in which thermal relaxation time is either of the same order or even lower than the pulsation period. The accurate determination of the eigenfunctions in these layers will therefore require the use of a non-adiabatic description which includes the entire atmosphere. This procedure then makes it possible to relate multicolor photometric observables with such eigenfunctions.

A number of authors (e.g., Dziembowski 1977a; Saio & Cox 1980; Pesnell 1990; Townsend 2002) have developed non-adiabatic codes and performed stellar pulsation calculations. However, these works have been carried out without a complete description of pulsation-atmosphere interaction.

In this paper two approaches are compared. The first follows Unno et al. (1989) for the equations and the numerical method used to solve them. Outer boundary conditions are imposed at the level of the photosphere. This approximation will be referred to below as "without atmosphere". The second applies a non-adiabatic pulsational treatment to the atmosphere derived by Dupret et al. (2002). This treatment has made it possible to obtain photometric observable values that are more realistic when compared with those generated by the "without" atmosphere approximation (referred to below as "with atmosphere"). The latter approach allows theoretical predictions to

Send offprint requests to: A. Moya, e-mail: moya@iaa.es
⋆ Marie Curie Postdoctoral Fellow, European Union.

be more directly connected with photometric observations than they previously had been by using only period comparisons.

Theoretical and observed amplitude ratios and phase differences can be compared as observed in different color photometric bands. Garrido et al. (1990) showed that the wavelength dependence of the limb darkening integrals is very weak for low l values. Thus, at least three color combinations, distributed in the widest possible range of wavelengths, give consistent values for phase lag ϕ^{T} and R. The latter parameter was defined by Watson (1988) and designed to measure departures from adiabatic conditions. Comparisons between non-adiabatic predictions and multicolor photometric observations have been made by Cugier et al. (1994) for β Cephei stars, Balona & Evers (1999) for δ Scuti stars and Townsend (2002) for Slowly Pulsating B stars. However, such comparisons were made without carrying out a detailed non-adiabatic pulsation treatment for the atmosphere. Photometric magnitude variations have been reformulated by Dupret et al. (2003), thus making it possible to obtain theoretical non-adiabatic quantities which explicitly include the atmosphere (Dupret et al. 2002). This reformulation has been employed in the study of β Cephei and Slowly Pulsating B stars.

In the present paper the approach of Dupret et al. (2002, 2003) is applied to δ Scuti stars. Non-adiabatic theoretical models "with" and "without" atmosphere, as well as their resolution algorithms, are presented. Solutions are compared in order to show the improvement introduced by including the pulsation-atmosphere interaction. One possible procedure for mode identifications using multicolor photometric diagrams is also suggested. For δ Scuti stars, the non-adiabatic observables with which we are working can be directly related with the characteristics of their thin convective envelopes. These envelopes are described by the Mixing Length Theory (MLT) and parametrized by α, which is defined as the proportionality constant relating the mean path of a convective element with local pressure scale height. The α parameter can be constrained by searching for the best fit between theoretical and observed photometric amplitude ratios and phase differences in color photometric bands. Such observables also depend on the opacity variation in the HeII, HeI and HI ionization zones.

2. Theoretical models

Equilibrium stellar models have been computed using the CESAM code (Morel 1997). In this code, the stellar atmosphere is described: 1) as a single layer (i.e., the photosphere) calculated in the Eddington approximation, or 2) using the Kurucz equilibrium atmospheric models (Kurucz 1993) to reconstruct the atmosphere from a specific Rosseland optical depth until reaching the last edge of the star. Table 1 shows the global characteristics of the equilibrium models. In the convective core of these models, overshooting has been set to 0.2 times the local pressure scale height.

The pulsational code begins by computing the adiabatic solution for fixed values of n and l, and this computation is used as trial input for the non-adiabatic computations "with" or "without" atmosphere. These calculations then make it possible to derive ϕ^{T}, $|\delta T_{\mathrm{eff}}/T_{\mathrm{eff}}|$ and $\delta g_{\mathrm{e}}/g_{\mathrm{e}}$, which are directly related to the photometric color variations.

Table 1. Global characteristics of the equilibrium models.

$\frac{M}{M_\odot}$	$\log T_{\mathrm{eff}}$	$\log g$	$\log \frac{L}{L_\odot}$	$\log \frac{R}{R_\odot}$	X_{c}
2.0	3.941	4.181	1.273	1.900	0.55
2.0	3.879	3.845	1.367	2.799	0.25
1.8	3.889	4.064	1.138	2.063	0.44

2.1. Non-adiabatic models "without" atmosphere

Here the adiabatic and non-adiabatic equations have been derived following Unno et al. (1989). However, two variables regarding the stellar interior have been modified in order to directly link the interior and atmosphere pulsation equations. These variables are

$$y_1 = \frac{\xi_{\mathrm{r}}}{r} \qquad y_2 = \frac{\delta P_{\mathrm{g}}}{P_{\mathrm{g}}} \qquad y_3 = \frac{\Phi'}{gr}$$
$$y_4 = \frac{\mathrm{d}\,\Phi'}{g\,\mathrm{d}r} \qquad y_5 = \frac{\delta T}{T} \qquad y_6 = \frac{\delta L_{\mathrm{R}}}{L_{\mathrm{R}}} \tag{1}$$

where ξ_{r} is the radial displacement, P_{g}, the gas pressure, Φ, the gravitational potential, L_{R}, the radiative luminosity and δX (resp. X'), the Lagrangian (resp. Eulerian) perturbation of the X variable. The other symbols bear their usual meaning.

The linear non-adiabatic pulsation equations corresponding to these variables are described in Appendix A (Eqs. (A.1) to (A.6)), and are obtained by neglecting the effects of rotation and the magnetic field. The "frozen" convection flux approximation, $\delta L_{\mathrm{C}} = 0$ and $\boldsymbol{F}'_{\mathrm{C}_\perp} = 0$, has been chosen by following Unno et al. (1989). Boundary conditions are also taken from the same source. Internal conditions are described by Eqs. (A.9) to (A.11) in Appendix A. Surface conditions are given here because they are particularly relevant to the comparison of the "with atmosphere" (Sect. 2.2) and "without atmosphere" treatment results:

1. The mechanical boundary condition

$$\left(\frac{l(l+1)}{\omega^2} - 4 - \omega^2\right) y_1 - \beta\, y_2 + \left(\frac{l(l+1)}{\omega^2} - 1 - l\right) y_3 - \frac{4}{3}\frac{aT^4}{P}\, y_5 = 0. \tag{2}$$

2. The potential boundary condition

$$(l+1)\, y_3 + y_4 = 0. \tag{3}$$

3. The thermal boundary condition

$$2\, y_1 + 4\, y_5 - y_6 = 0. \tag{4}$$

Note that Eq. (4) is obtained by perturbing the equation which defines the effective temperature ($L_{\mathrm{R}} = 4\pi R^2 \sigma_{\mathrm{rad}}\, T_{\mathrm{eff}}^4$), as well as by assuming that in the photosphere:

$$\frac{\delta T}{T} = \frac{\delta T_{\mathrm{eff}}}{T_{\mathrm{eff}}}. \tag{5}$$

2.2. Non-adiabatic models "with" atmosphere

Equations (A.1)–(A.6) are also used to describe the pulsation inside the star, whereas Eqs. (A.9)–(A.11) describe the internal boundary conditions. However, the complete atmosphere pulsation equations are solved following Dupret et al. (2002). The latter equations have been derived by taking into account that: 1) the radiation field is not isotropic in the atmosphere and the diffusion approximation is therefore not valid in this case; and 2) the radiation stress tensor cannot be represented by a diagonal matrix with a constant element: $P_{\rm R} = (1/3)aT^4$.

For these reasons, new approximations have been used with respect to those solved for the interior in order to obtain an improved description of the atmosphere. This new approach is based on the fact that the atmosperic thermal relaxation time is very short as compared to pulsation periods. Consequently, it can be assumed that during each pulsation period, the atmosphere remains in thermal equilibrium. Rewriting the equations given in Dupret et al. (2002), those corresponding to the atmosphere are:

$$x\frac{{\rm d}y_1}{{\rm d}x} = \left(\frac{l(l+1)}{c_1\omega^2} - 3\right)y_1 + \left(\frac{l(l+1)}{c_1\omega^2}\frac{P_{\rm g}}{\rho g r} - \frac{1}{P_{{\rm g}\rho}}\right)y_2 + \frac{l(l+1)}{c_1\omega^2}\,y_3 + \left(\frac{P_{\rm gT}}{P_{{\rm g}\rho}} + \frac{l(l+1)}{c_1\omega^2}\frac{a_{\rm R}}{\nabla g V}\right)y_5 \quad (6)$$

$$x\frac{{\rm d}y_2}{{\rm d}x} = \frac{\rho g r}{P_{\rm g}}\left(c_1\omega^2 - U + 2 + \left(\frac{a_{\rm R}}{g} - 1\right)\left(\frac{l(l+1)}{c_1\omega^2} - 2\right)\right)y_1 + \frac{\rho g r}{P_{\rm g}}\left(\left(\frac{a_{\rm R}}{g} - 1\right)\left(\frac{l(l+1)}{c_1\omega^2}\frac{P_{\rm g}}{\rho g r} - 1\right) + \frac{a_{\rm R}}{g}\frac{\kappa_\rho}{P_{{\rm g}\rho}}\right)y_2 + \left(\frac{a_{\rm R}}{g} - 1\right)\frac{l(l+1)}{c_1\omega^2}\frac{\rho g r}{P_{\rm g}}\,y_3 - \frac{\rho g r}{P_{\rm g}}\,y_4 + \frac{\rho g r}{P_{\rm g}}\left(\left(\frac{a_{\rm R}}{g} - 1\right)\times\frac{l(l+1)}{c_1\omega^2}\frac{a_{\rm R}}{\nabla g V} + \frac{a_{\rm R}}{g}\left(\kappa_{\rm T} - \kappa_\rho\frac{P_{\rm gT}}{P_{{\rm g}\rho}}\right)\right)y_5 + 4\frac{\rho r a_{\rm R}}{P_{\rm g}}\frac{\delta T_{\rm eff}}{T_{\rm eff}} \quad (7)$$

$$x\frac{{\rm d}y_3}{{\rm d}x} = \left(1 - U\right)y_3 + y_4 \quad (8)$$

$$x\frac{{\rm d}y_4}{{\rm d}x} = -U\frac{{\rm d}\ln\rho}{{\rm d}\ln r}\,y_1 + \frac{U}{P_{{\rm g}\rho}}\,y_2 + l(l+1)\,y_3 - U\,y_4 - U\frac{P_{\rm gT}}{P_{{\rm g}\rho}}\,y_5 \quad (9)$$

$$x\frac{{\rm d}y_5}{{\rm d}x} = -\frac{\kappa\rho r}{\tau}\frac{\partial\ln T}{\partial\ln\tau}\left(\frac{l(l+1)}{c_1\omega^2} - 2\right)y_1 - \frac{\kappa\rho r}{\tau}\frac{\partial\ln T}{\partial\ln\tau}\left(\frac{\kappa_\rho}{P_{{\rm g}\rho}} + \frac{l(l+1)}{c_1\omega^2}\frac{P_{\rm g}}{\rho g r}\right)y_2 - \frac{\kappa\rho r}{\tau}\frac{\partial\ln T}{\partial\ln\tau}\frac{l(l+1)}{c_1\omega^2}\,y_3 - \frac{\kappa\rho r}{\tau}\left(\frac{\partial\ln T}{\partial\ln\tau}\left(\kappa_{\rm T} - \kappa_\rho\frac{P_{\rm gT}}{P_{{\rm g}\rho}}\frac{l(l+1)}{c_1\omega^2}\frac{a_{\rm R}}{\nabla g V}\right) - 1 + \left(\frac{\partial^2\ln T}{\partial\ln\tau^2}\right)\Big/\left(\frac{\partial\ln T}{\partial\ln\tau}\right)\right)y_5 - \frac{\kappa\rho r}{\tau}\left[\left(1 - \left(\frac{\partial^2\ln T}{\partial\ln\tau^2}\right)\Big/\left(\frac{\partial\ln T}{\partial\ln\tau}\right)\right)\times\left(\frac{\partial\ln T}{\partial\ln T_{\rm eff}}\frac{\delta T_{\rm eff}}{T_{\rm eff}} + \frac{\partial\ln T}{\partial\ln g_{\rm e}}\frac{\delta g_{\rm e}}{g_{\rm e}}\right) + \frac{\partial^2\ln T}{\partial\ln\tau\partial\ln T_{\rm eff}}\frac{\delta T_{\rm eff}}{T_{\rm eff}} + \frac{\partial^2\ln T}{\partial\ln\tau\partial\ln g_{\rm e}}\frac{\delta g_{\rm e}}{g_{\rm e}}\right] \quad (10)$$

$$x\frac{{\rm d}y_6}{{\rm d}x} = 0 \quad (11)$$

where the new variables are defined as:

$$P_{\rm g}(\text{or}\,\kappa)_\rho = \left.\frac{\partial\ln P_{\rm g}\,(\text{or}\,\kappa)}{\partial\ln\rho}\right|_{\rm T} \qquad P_{\rm g}\,(\text{or}\,\kappa)_{\rm T} = \left.\frac{\partial\ln P_{\rm g}(\text{or}\,\kappa)}{\partial\ln T}\right|_\rho \quad (12)$$

and where $a_{\rm R}$ is the radiative acceleration and τ the Rosseland optical depth. The atmospheric equilibrium quantities for these equations have been obtained from the Kurucz model atmospheres (Kurucz 1993).

In comparison to those used for the "without" atmosphere treatment, the boundary conditions for these equations are:

1. The mechanical boundary condition is obtained by neglecting the derivative of the gas pressure perturbation at the stellar surface:

$$x\frac{{\rm d}\,y_2}{{\rm d}x} = 0. \quad (13)$$

Inserting Eq. (13) in Eq. (7):

$$\left(c_1\omega^2 - U + 2 + \left(\frac{a_{\rm R}}{g} - 1\right)\left(\frac{l(l+1)}{c_1\omega^2} - 2\right)\right)y_1 + \left(\left(\frac{a_{\rm R}}{g} - 1\right)\left(\frac{l(l+1)}{c_1\omega^2}\frac{P_{\rm g}}{\rho g r} - 1\right) + \frac{a_{\rm R}}{g}\frac{\kappa_\rho}{P_{{\rm g}\rho}}\right)y_2 + \left(\frac{a_{\rm R}}{g} - 1\right)\frac{l(l+1)}{c_1\omega^2}\,y_3 - y_4 + \left(\left(\frac{a_{\rm R}}{g} - 1\right)\frac{l(l+1)}{c_1\omega^2}\frac{a_{\rm R}}{\nabla g V} + \frac{a_{\rm R}}{g}\left(\kappa_{\rm T} - \kappa_\rho\frac{P_{\rm gT}}{P_{{\rm g}\rho}}\right)\right)y_5 + 4\frac{a_{\rm R}}{g}\frac{\delta T_{\rm eff}}{T_{\rm eff}} = 0. \quad (14)$$

2. The potential boundary condition remains the same:

$$(l+1)\,y_3 + y_4 = 0. \quad (15)$$

3. The thermal boundary condition, following Dupret et al. (2002):

$$\frac{\partial\ln T}{\partial\ln T_{\rm eff}}\frac{\delta T_{\rm eff}}{T_{\rm eff}} + \frac{\partial\ln T}{\partial\ln g_{\rm e}}\frac{\delta g_{\rm e}}{g_{\rm e}} + \frac{\partial\ln T}{\partial\ln\tau}\left(\frac{l(l+1)}{c_1\omega^2} - 2\right)y_1 + \frac{\partial\ln T}{\partial\ln\tau}\left(\frac{\kappa_\rho}{P_{{\rm g}\rho}} + \frac{l(l+1)}{c_1\omega^2}\frac{P_{\rm g}}{\rho g r}\right)y_2 + \frac{\partial\ln T}{\partial\ln\tau}\frac{l(l+1)}{c_1\omega^2}\,y_3 + \left(\frac{\partial\ln T}{\partial\ln\tau}\left(\kappa_{\rm T} - \kappa_\rho\frac{P_{\rm gT}}{P_{{\rm g}\rho}} + \frac{l(l+1)}{c_1\omega^2}\frac{a_{\rm R}}{\nabla g V}\right) - 1\right)y_5 = 0. \quad (16)$$

A connecting layer is required which marks the border between the interior (Eqs. (A.1) to (A.6)) and atmosphere treatments (Eqs. (6) to (11)). The boundary conditions for the equilibrium models are calculated at the same connecting layer by imposing an adequate match with the Kurucz model atmosphere (Kurucz 1993). Two restrictions are imposed in order to choose the location of this layer: 1) the diffusion approximation must be valid and 2) the layer must be located outside the convective envelope, since the atmospheric non-adiabatic treatment is not justified inside a convection zone, and because consistency requirements exist between the interior and atmosphere treatments.

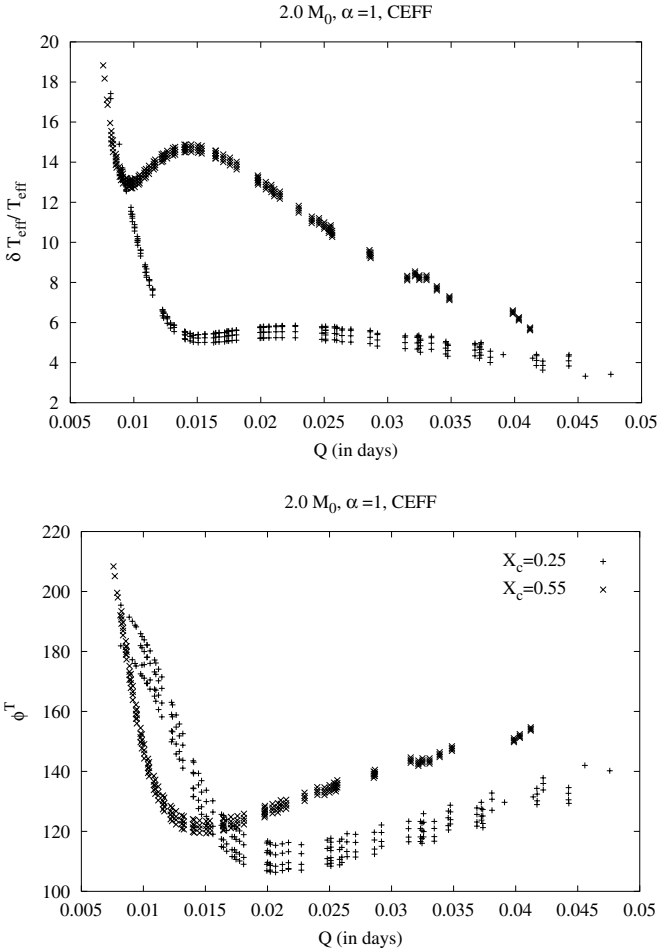

Fig. 1. Non-adiabatic quantities $|\delta T_{\rm eff}/T_{\rm eff}|$ (*top*) and $\phi^{\rm T}$ (*bottom*), as a function of the pulsation constant Q (in days) for different modes with spherical degrees $l = 0, 1, 2, 3$. Two 2.0 $M_\odot$ models are solved at different evolutionary phases, with a MLT parameter $\alpha = 1$ and the CEFF equation of state. Different values correspond to different locations of the connecting layer: $\tau = 1, 1.1, 1.2, 1.3$. "+" are for the model with $X_{\rm c} = 0.25$ and "×" for $X_{\rm c} = 0.55$.

One of the uncertainties of the "with" atmosphere global algorithm is the location of the optical depth in which this connecting layer is defined, being that, despite the above-mentioned constraints, a small set of possible locations still exists. Figure 1 shows the non-adiabatic results for two 2 $M_\odot$ stellar models at different evolutionary stages, locating the connecting layer at $\tau = 1, 1.1, 1.2$ and 1.3. Note that these results are not significantly affected by this choice. The connecting layer is selected at $\tau = 1$.

The two additional variables $\delta T_{\rm eff}$ and $\delta g_{\rm e}$ can be derived from:

$$4\frac{\delta T_{\rm eff}}{T_{\rm eff}} = y_6 - 2\,y_1 \tag{17}$$

$$\frac{\delta g_{\rm e}}{g_{\rm e}} = y_4 + \Big(U - 2 - c_1\omega^2\Big)y_1. \tag{18}$$

These quantities are determined at the photosphere ($\log T = \log T_{\rm eff}$). The results are not significantly sensitive to the choice of this layer: a slight change of location implies changes which are always smaller than 5 percent for $|\delta T_{\rm eff}/T_{\rm eff}|$, smaller than 1 degree for the phase-lag $\phi^{\rm T}$ and which are negligible for $\delta g_{\rm e}/g_{\rm e}$.

3. Multicolor photometry

An important application of our non-adiabatic code is that its theoretical predictions can be tested against multicolor photometric observations. The non-adiabatic quantities $|\delta T_{\rm eff}/T_{\rm eff}|$, $\delta g_{\rm e}/g_{\rm e}$ and $\phi^{\rm T}$ can be related to the photometric observables: amplitude ratios and phase differences between filters. In a one-layer linear approximation, the monochromatic magnitude variation of a non-radially pulsating star is given by:

$$\begin{aligned}\delta m_\lambda = -\frac{2.5}{\ln 10}\, a\, P_l^m(\cos i)\, b_{l\lambda}\Big[&-(l-1)(l+2)\cos(\sigma t)\\ &+f_{\rm T}\cos(\sigma t+\phi^{\rm T})(\alpha_{{\rm T}\lambda}+\beta_{{\rm T}\lambda})\\ &-f_{\rm g}\cos(\sigma t)(\alpha_{{\rm g}\lambda}+\beta_{{\rm g}\lambda})\Big]\end{aligned} \tag{19}$$

where

$$b_{l\lambda} = \int_0^1 h_\lambda\, \mu P_l\, {\rm d}\mu \tag{20}$$

$$\alpha_{{\rm T}\lambda} = \frac{\partial \ln F_\lambda^+}{\partial \ln T_{\rm eff}}; \qquad \alpha_{{\rm g}\lambda} = \frac{\partial \ln F_\lambda^+}{\partial \ln g_{\rm e}} \tag{21}$$

$$\beta_{{\rm T}\lambda} = \frac{\partial \ln b_{l\lambda}}{\partial \ln T_{\rm eff}}; \qquad \beta_{{\rm g}\lambda} = \frac{\partial \ln b_{l\lambda}}{\partial \ln g_{\rm e}} \tag{22}$$

$$f_{\rm T} = \left|\frac{\delta T_{\rm eff}}{T_{\rm eff}}\right|; \qquad f_{\rm g} = \left|\frac{\delta g_{\rm e}}{g_{\rm e}}\right| \tag{23}$$

$f_{\rm T}$ and $f_{\rm g}$ are the relative amplitudes of local effective temperature and gravity variations for a normalized radial displacement at the photosphere, $\phi^{\rm T}$ is the phase difference between the relative effective temperature variation and the relative radial displacement and σ is the pulsation frequency. a corresponds to the real amplitude of the relative radial displacement, P_l^m is the associated Legendre function and i the inclination angle between the stellar rotation axis and the observer line of sight.

One appropriate way to test multicolor theoretical predictions is to construct phase-amplitude diagrams corresponding to well-chosen combinations of photometric bands. In these diagrams the theoretical results corresponding to modes of different spherical degrees ℓ occupy well differentiated regions. This enables the identification of ℓ by searching for the best fit between theory and observations. As is shown in Sect. 4, the non-adiabatic quantities $f_{\rm T}$, $f_{\rm g}$ and $\phi^{\rm T}$, which play a major role in Eq. (19), are highly sensitive to the characteristics of the convective envelope. The confrontation between the theoretical and observed amplitude ratios and phase differences can thus be used to constrain the physical conditions of this convection zone.

4. Applications to δ Scuti stars

As a prerequisite to the presentation of the "with" atmosphere treatment results, of particular interest is that the differences be analized between the non-adiabatic observables appearing as a consequence of "with" and "without" atmosphere descriptions. In Fig. 2 these differences are displayed for a 1.8 $M_\odot$

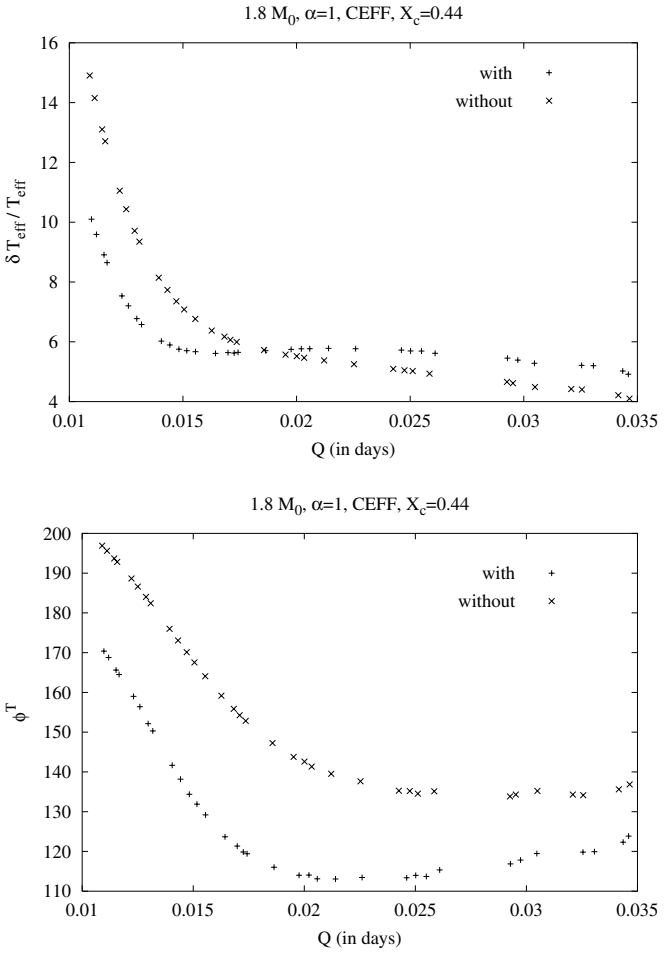

Fig. 2. Non-adiabatic quantities $|\delta T_{\rm eff}/T_{\rm eff}|$ (*top*) and $\phi^{\rm T}$ (*bottom*), as a function of the pulsation constant Q (in days) for different modes with spherical degrees $l = 0, 1, 2, 3$. A model of a 1.8 $M_\odot$ is solved with $X_{\rm c} = 0.44$, a MLT parameter $\alpha = 1$ and the CEFF equation of state. Results obtained "with" (+) and "without" atmosphere (×) in the non-adiabatic treatment are compared.

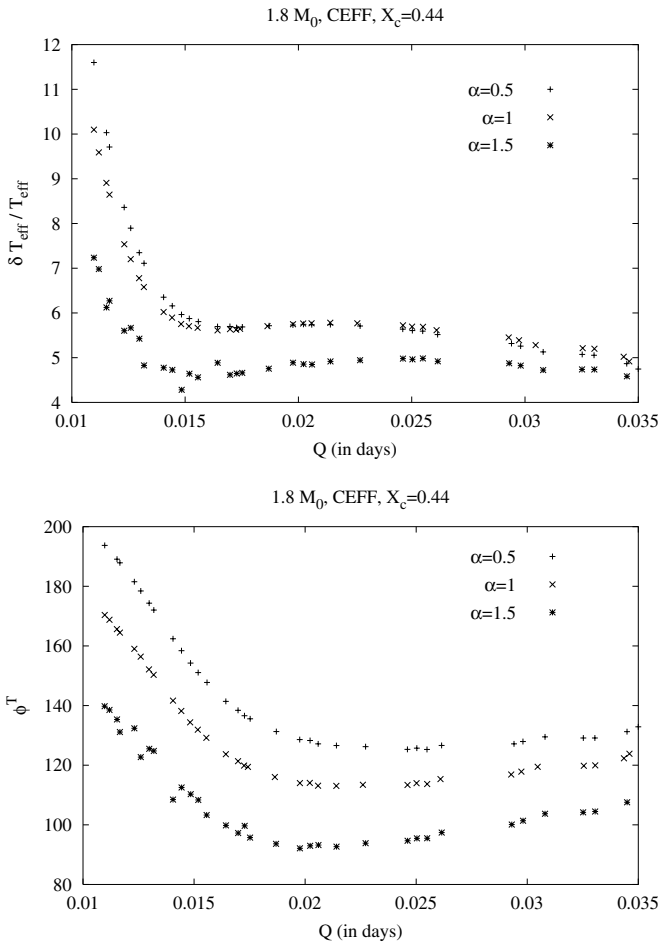

Fig. 3. Non-adiabatic quantities $|\delta T_{\rm eff}/T_{\rm eff}|$ (*top*) and $\phi^{\rm T}$ (*bottom*), as a function of the pulsation constant Q (in days) for different modes with spherical degrees $l = 0, 1, 2, 3$. Models of 1.8 $M_\odot$ are solved with $X_{\rm c} = 0.44$ and with different values for the MLT parameter: $\alpha = 0.5, 1, 1.5$. Note the sensitivity of the non-adiabatic results with respect to α.

model in the middle of the evolutionary phase ($X_{\rm c} = 0.44$) towards the exhaustion hydrogen in the core. For the relative amplitude of the local effective temperature variation, the effect of introducing the atmospheric treatment is slight, though significant, especially around the overstable modes (between $Q = 0.02$ and $Q = 0.012$ days in this model). However, the phase lag $\phi^{\rm T}$ is more sensitive to this treatment for all frequencies and displays a mean difference of 30° for the overstable modes. As of the latter modes, these quantities increase with the frequency. It should be noted that the differences in $|\frac{\delta g_{\rm e}}{g_{\rm e}}|$ between the "with" and "without" atmosphere models are negligible. Furthermore, it should be stressed that the frequencies obtained using both treatments are almost identical, i.e., the only difference between the two treatments appears in the outermost layers, and this has no effect on the frequency results. In Fig. 2 it can be seen that the non-adiabatic results for a fixed model are independent of the spherical degree l for p-modes.

Only pulsation models "with" atmosphere will be considered in what follows. In Fig. 3 non-adiabatic results are compared as obtained for models of 1.8 $M_\odot$ and $X_{\rm c} = 0.44$, and with different values for the MLT parameter ($\alpha = 0.5, 1, 1.5$). The non-adiabatic quantities $|\delta T_{\rm eff}/T_{\rm eff}|$ and $\phi^{\rm T}$ are significantly affected by the value of α, especially the phase lag. A more detailed description of the sensitivity of the non-adiabatic results to α is given in Fig. 4. This figure displays the ratio between radiative and total luminosity (top), the convective efficiency (middle) and the luminosity phase lag $\phi_{\rm L} = \phi\left(\frac{\delta L}{L}\right) - \phi\left(\frac{\xi_{\rm r}}{r}\right)$ (bottom panel), all three as a function of the logarithm of temperature. Note that $\phi_{\rm L}$ closely follows $\phi^{\rm T}$ at the photosphere throughout Eq. (17).

The bottom panel of Fig. 4 shows that along the radius of the star there are two zones in which a phase lag is introduced: the first located in the partial ionization zone of HeII and the second, in the surface convection zone (partial HI and HeI ionization). In this panel it can also be seen that the the phase lag sensitivity to α appears in the surface convection zone.

The convective efficiency in MLT, defined as

$$\Gamma = \left[\frac{4}{9}\left(\frac{c_{\rm p}\kappa p\rho c_{\rm s}\alpha^2}{9\sigma_{\rm steff}T^3 g\sqrt{2\Gamma_1}}\right)^2(\nabla_{\rm rad}-\nabla)\right]^{\frac{1}{3}} \tag{24}$$

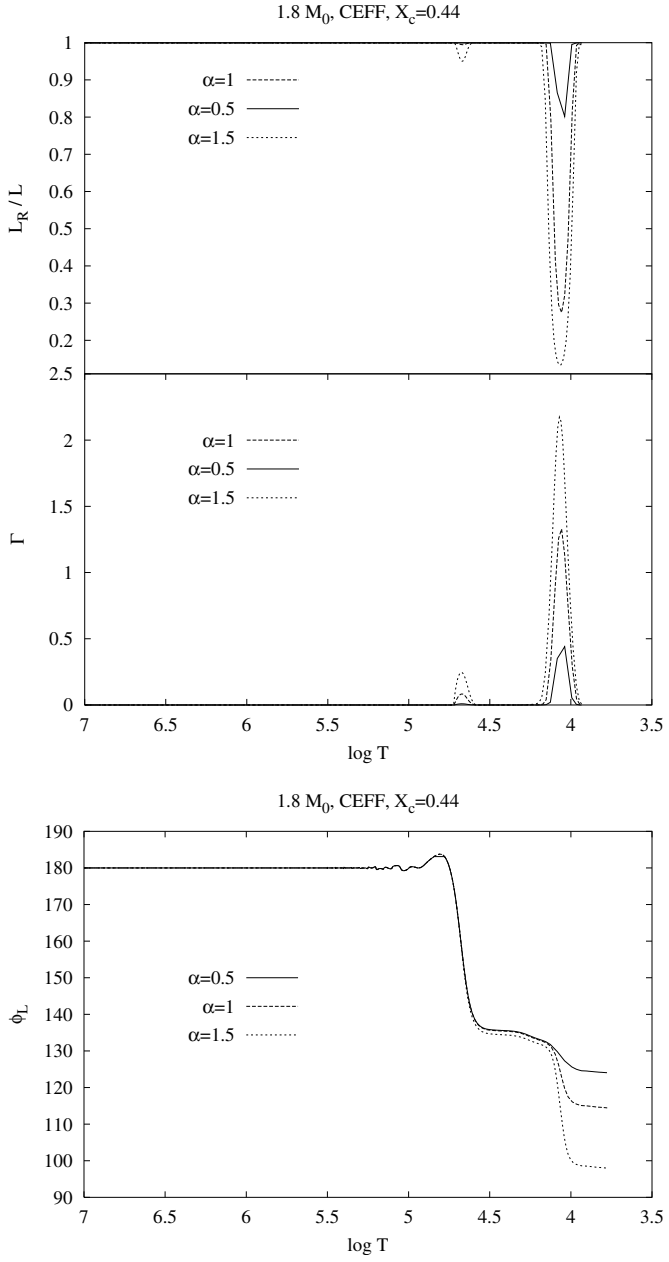

Fig. 4. Radiative luminosity over total luminosity (*top panel*), convective efficiency (*middle panel*) and the luminosity phase lag $\phi_{\rm L} = \phi\left(\frac{\delta L}{L}\right) - \phi\left(\frac{\xi_{\rm r}}{r}\right)$ (*bottom panel*) as a function of the logarithm of temperature, for the fundamental radial mode. 1.8 $M_\odot$ models are solved with $X_{\rm c} = 0.44$, and three different values of the MLT parameter: $\alpha = 0.5, 1, 1.5$. Note the differences appearing in the superficial convection zone as α values rise.

(Cox 1980), and the convection zone temperature gradient are both directly linked to α. Phase-lags originate in the energy conservation equation due to the introduction of explicitly imaginary parts. For a radial mode, and freezing the convective luminosity, the equations are:

$$i\sigma T\delta S = \delta\epsilon_{\rm N} - \frac{{\rm d}\delta L_{\rm R}}{{\rm d}M_{\rm r}} \tag{25}$$

where $M_{\rm r}$ is the mass enclosed in a sphere of radius r, and

$$\frac{\delta L_{\rm R}}{L_{\rm R}} = -\frac{\delta\kappa}{\kappa} + 4\frac{\xi_{\rm r}}{r} + 4\frac{\delta T}{T} + \frac{{\rm d}\frac{\delta T}{T}/{\rm d}\ln r}{{\rm d}\ln T/{\rm d}\ln r}\cdot \tag{26}$$

Phase-lags originate mainly through the interplay between the different terms of Eq. (26), which affect the right hand side of Eq. (25) only when the thermal relaxation time is sufficiently small. A first phase-lag is introduced in the partial ionization zone of HeII (bottom panel of Fig. 4). The partial ionization produces an opacity bump and a considerable decrease in the adiabatic exponents. This significantly affects $\delta\kappa/\kappa$. A second source of phase lag occurs in the surface convective zone (partial ionization zone of HI and HeI). In this case variations in α primarily influence the temperature gradient and the size of the convective zone. The latter two then affect the phase-lag throughout the above equations.

As is shown in Fig. 1, the non-adiabatic results are highly sensitive to the evolutionary phase of the star. As the star evolves in the HR diagram, changes in these quantities are larger for the relative variations of the effective temperature than for the phase lags. Changes in the evolution phase do not qualitatively affect the non-adiabatic results in the same manner as do changes in α. In the latter case, only the characteristics of the convective zone are influenced. In contrast, changes in the evolution phase have an effect on both the characteristics of the superficial convective zone and the position of the HeII partial ionization zone.

Figure 5 is obtained by plotting the phase lag and $|\delta T_{\rm eff}/T_{\rm eff}|$ versus $\log T_{\rm eff}$ for the fundamental radial mode of two complete tracks of 2.0 $M_\odot$ and 1.8 $M_\odot$ stars. Three values of the MLT parameter α (1.5, 1.0 and 0.5) have been used. When stellar temperatures are high enough to originate a negligible external convective zone, the values are independent of α; this only occurs for the 2.0 $M_\odot$ models presented. For cooler models, however, convection becomes more efficient, thus producing different phase lags and relative effective temperature variations for similar effective temperatures (Balona & Evers 1999).

Figure 4 refers to the behaviour of these phase lags. Each step in the figure makes it possible to view the phase lag, $\phi^{\rm T}$, as the sum of two phases ($\phi_{\rm L} = \phi_\kappa + \phi_{\rm conv}$). The latter can be referred to as the κ-phase ($\phi_\kappa \equiv$ phase difference between 180° and $\phi_{\rm L}$ (at $\log T = 4.5$)) and the convective-phase ($\phi_{\rm conv} \equiv$ phase difference between $\phi_{\rm L}$ (at $\log T = 4.5$) and $\phi_{\rm L}$ (at $\log T = \log T_{\rm eff}$)). Figure 6 is obtained by plotting both versus $\log T_{\rm eff}$.

The κ-phase lag ϕ_κ displays a behaviour which is directly related to the position of the model in the HR diagram and which is independent of the α parameter. Therefore, ϕ_κ shows the contribution of only one of the phase sources, the opacity variation, since convection is not efficient in this part of the star.

The contribution to the convection zone phase, in this case $\phi_{\rm conv}$, is in turn a sum of two phase sources. For hot models the κ driving mechanism is not yet efficient enough to introduce a phase lag, and the behaviour of $\phi_{\rm conv}$ depends mainly on the convection treatment. When the convective layers are not efficient, models with different values of α produce the same values of $\phi_{\rm conv}$. At $\log T_{\rm eff} \approx 3.91$ the convective layers become sufficiently efficient to distinguish between models using different values of α, independently of the mass. From

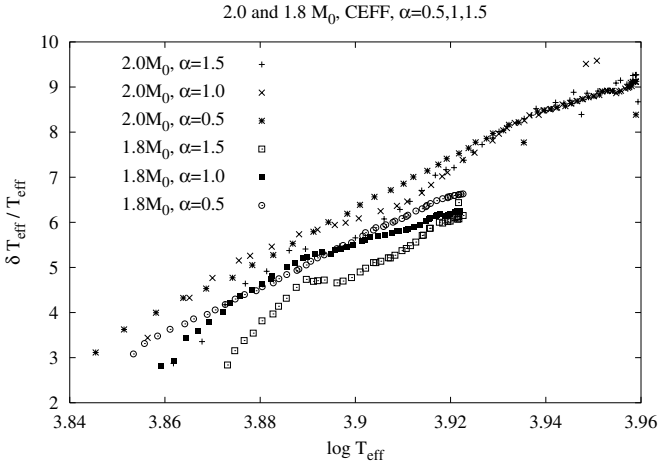

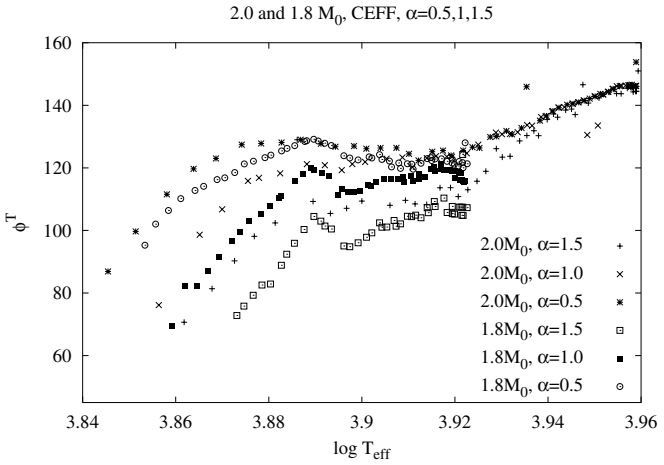

Fig. 5. Non-adiabatic quantities $|\delta T_{\rm eff}/T_{\rm eff}|$ (*top*) and $\phi^{\rm T}$ (*bottom*) as a function of $\log T_{\rm eff}$ for the fundamental radial mode in two complete tracks of 2.0 $M_\odot$ and 1.8 $M_\odot$ stars for three different values of the MLT parameter α =1.5,1 and 0.5.

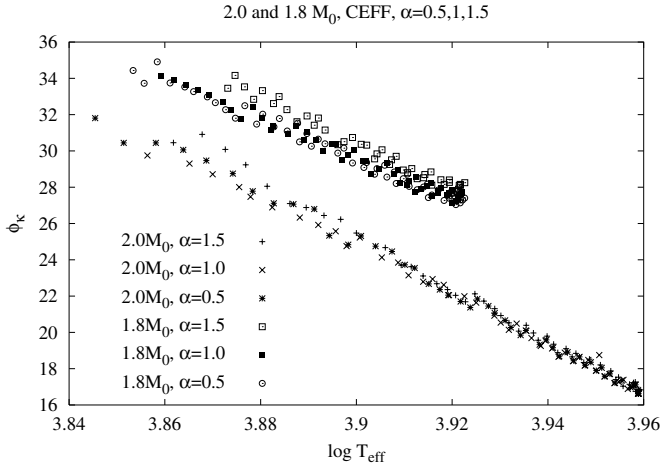

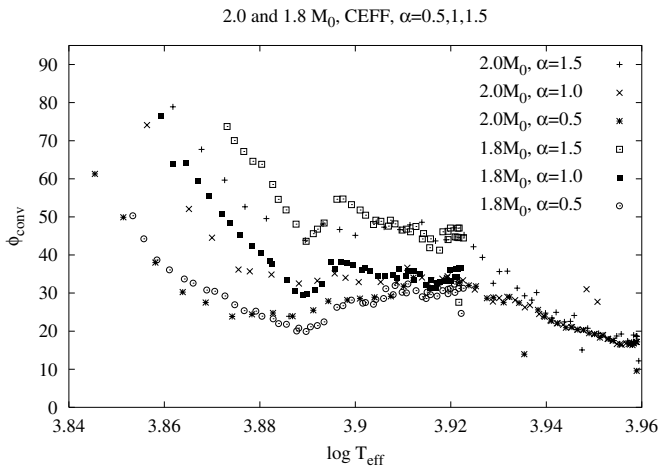

Fig. 6. κ-phase ϕ_κ (*top*) and convective-phase $\phi_{\rm conv}$ (*bottom*) as a function of $\log T_{\rm eff}$ for the fundamental radial mode in two complete tracks of 2.0 $M_\odot$ and 1.8 $M_\odot$ stars for three different values of the MLT parameter α = 1.5, 1.0 and 0.5.

$\log T_{\rm eff}$ = 3.88 to cooler models, an increase is observed in the value of this phase lag, again displaying different behaviours for different masses and values of α. This is accounted for by the fact that, within this range of temperature, the κ driving mechanism in the HI and HeI ionization zone becomes efficient enough to make a significant contribution to $\phi_{\rm conv}$.

Figure 7 is obtained by displaying $|\delta T_{\rm eff}/T_{\rm eff}|$ versus the integral of the convective efficiency, as defined in Eq. (24) for all models. The behaviour of these quantities can be distinguished independently of the mass of the model, which in this case is exclusively a function of the evolution phase and α.

5. Applications to multicolor photometry

All of the above-mentioned calculations have a direct influence on the phase difference – amplitude ratio diagrams. Now phase lags, as well as relative variations in $|\delta T_{\rm eff}/T_{\rm eff}|$ and $\delta g_{\rm e}/g_{\rm e}$, can be used to overcome the uncertainties in previous phase-ratio color diagrams. In Garrido (2000) these discrimination diagrams were made using parametrized values for departures from adiabaticity and phase lags. The only remaining degree of freedom is now the choice of the MLT α parameter in order

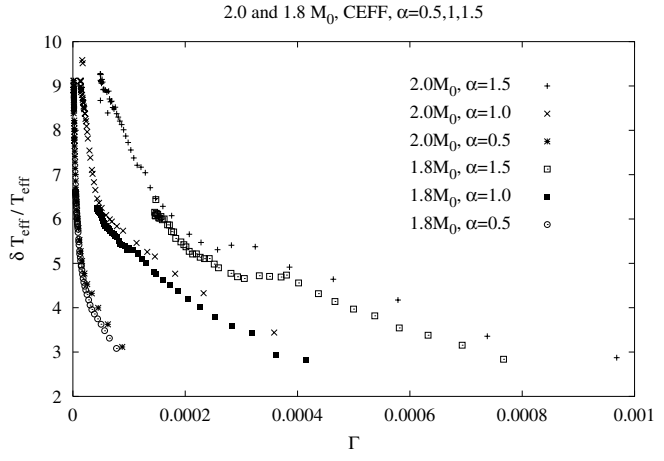

Fig. 7. $|\delta T_{\rm eff}/T_{\rm eff}|$ as a function of the integral of the convective efficiency Γ for the fundamental radial mode in two complete tracks of 2.0 $M_\odot$ and 1.8 $M_\odot$ stars for three different values of the MLT parameter α = 1.5, 1.0 and 0.5.

to describe the convection. Therefore, discrimination diagrams depend only on this parameter, as is shown in Fig. 8 where theoretical predictions are plotted for two specific Strömgren

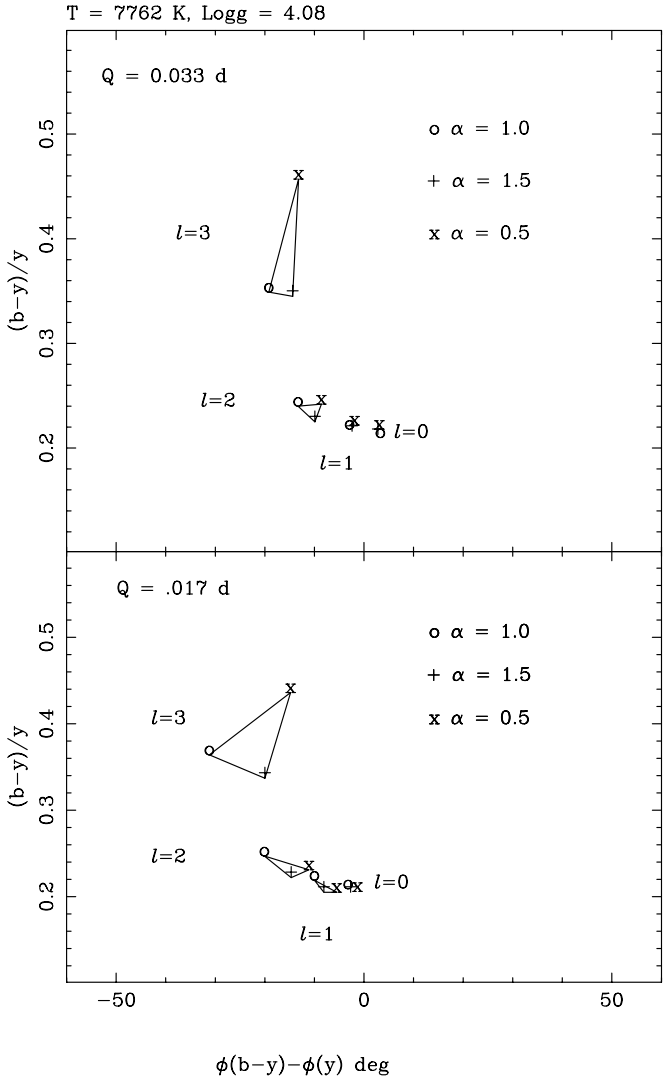

Fig. 8. The top panel shows theoretical predictions for two specific Strömgren photometric bands ($(b-y)$ and y) for a given theoretical model using three MLT α parameters in the fundamental radial mode regime (pulsation constant near 0.033 days). The 3rd overtone regime (pulsation constant near 0.017 days) is shown in the bottom panel.

photometric bands ($(b-y)$ and y) with a given theoretical model using three different MLT α parameters in the fundamental radial mode regime (pulsation constant near 0.033 days) and in the 3rd overtone regime (near 0.017 days).

A clear separation between the l-values exists for periods around the fundamental radial. Similar behaviour is found for other modes in the proximity of the 3rd radial overtone, although for these shorter periods some overlappings start to appear at the lowest l-values. They also show the same trend as in the fundamental radial mode: high amplitude ratios for low MLT α and the spherical harmonic $l = 3$. A more detailed description of these diagrams using different models and photometric bands will be given in a forthcoming paper.

6. Conclusions

This paper uses the CESAM package to generate equilibrium models. A new non-adiabatic pulsation code has been developed and applied to the study of δ Scuti stars. This code takes into account the stellar atmosphere in two ways: 1) as the boundary layer of the star ("without" atmosphere); in this case photospheric observables such as amplitudes and phases of both $T_{\rm eff}$ and gravity, reflect the boundary conditions we impose; and 2) particular consideration is given to pulsation treatment ("with" atmosphere), thus extending the star beyond the photosphere. As a consequence of applying the "with" atmosphere treatment, photospheric observables become determinable as a solution to a set of differential equations. These equations have been described by Dupret et al. (2002).

The non-adiabatic code presented in this paper enables the determination of the photometric observables $|\delta T_{\rm eff}/T_{\rm eff}|$, $|\delta g_{\rm e}/g_{\rm e}|$ and $\phi^{\rm T}$. The results of the "without" atmosphere approach strongly depend on the choice of external boundary conditions. In contrast, the "with" atmosphere approach only implies those uncertainties brought about by the physical assumptions imposed in order to obtain the differential equations.

The comparison of the results generated by both treatments shows that the values for $|\delta T_{\rm eff}/T_{\rm eff}|$ are relatively similar in most of the spectrum. However, differences become notable for shorter periods, in which "without" atmosphere solutions are larger than those of the "with" atmosphere treatment. Differences in $\phi^{\rm T}$ are significant and have a mean value of approximately 30° within the range of the periods studied. The non-adiabatic results presented here are highly sensitive to the characteristics of the superficial convective zone, parametrized by using the mixing length parameter α. In particular, we have shown that there are two regions in which the phase lag originates. A first phase lag takes place in the partial ionization zone of HeII, where the κ mechanism drives the oscillations. This phase lag is very sensitive to the evolution phase. A second one occurs in the convective envelope (partial ionization zone of HI and HeI) and is sensitive mainly to α. Though to a lesser extent, this phase lag is also sensitive to the evolutionary phase because of the κ driving mechanism and the size of the convection zone change.

In this paper it is shown that theoretical photometric amplitude ratios and phase differences are very sensitive to non-adiabatic calculations. The treatment and location of the outer boundary conditions, here referred to as "with" and "without" atmosphere, have been shown to give significantly different theoretical predictions. Consequently, our improved non-adiabatic treatment of the atmosphere will probably enable more accurate photometric mode identifications. Our results confirm the recent theoretical results of Daszyńska-Daszkiewicz et al. (2003) which show that phases and amplitudes in different colours are affected by the choice of the α parameter, although the authors calculated the model atmospheres in the Eddington approximation. By determining the best fit between theory and observations, it may thus be possible to constrain the MLT parameter α.

Acknowledgements. This work was partialy financed by program ESP 2001-4528-PE. The authors are also grateful to Marco Bettini for thorough editing of the original English manuscript.

Appendix A: Stellar interior equations and inner boundary conditions

These equations have been developed following Unno et al. (1989). Eigenfunctions $\frac{1}{gr}\left(\frac{p'}{\rho}+\Phi'\right)$ and $\frac{\delta S}{c_p}$ have been replaced by $\frac{\delta P_g}{P_g}$ and $\frac{\delta T}{T}$ to adapt the equations to the atmospheric ones. This was done to make the transition in the connecting layer as smooth as possible. Having introduced these modifications, the nonadiabatic nondimensional equations for the stellar interior are

$$\begin{aligned} x\frac{\mathrm{d}y_1}{\mathrm{d}x} &= \left(\frac{l(l+1)}{c_1\omega^2}-3\right)y_1 \\ &+\left(\frac{l(l+1)}{c_1\omega^2}-V_g-\nabla_{ad}\,V\,\upsilon_T\right)\frac{\beta}{V}\,y_2+\frac{l(l+1)}{c_1\omega^2}\,y_3 \\ &+\left[\frac{4}{3}\frac{aT^4}{PV}\left(\frac{l(l+1)}{c_1\omega^2}-V_g-\nabla_{ad}\,V\,\upsilon_T\right)+\upsilon_T\right]y_5 \qquad (A.1) \\ x\frac{\mathrm{d}y_2}{\mathrm{d}x} &= \frac{V}{\beta}\left(c_1\omega^2-U+\left(4-\frac{l(l+1)}{c_1\omega^2}\right)\left(1-\frac{4}{3}\frac{aT^4}{P}\nabla\right)\right)y_1 \\ &+\left[\frac{V}{\beta}\left(1-\frac{4}{3}\frac{aT^4}{P}\nabla\right)-\frac{l(l+1)}{c_1\omega^2}\right. \\ &\left.-\frac{4}{3}\frac{aT^4}{P}\left[V\,\nabla\left(\nabla_{ad}\kappa_S-\kappa_{ad}\right)-\nabla\frac{l(l+1)}{c_1\omega^2}\right]\right]y_2 \\ &+\frac{V}{\beta}\,\frac{l(l+1)}{c_1\omega^2}\left(\frac{4}{3}\frac{aT^4}{P}\nabla-1\right)y_3-\frac{V}{\beta}\,y_4 \\ &-\frac{4}{3}\frac{aT^4}{P\beta}\left[4\nabla+\frac{l(l+1)}{c_1\omega^2}+V\,\nabla\left(4-\kappa_S\right)\right. \\ &\left.+\frac{4}{3}\frac{aT^4}{P}\left[V\,\nabla\left(\nabla_{ad}\kappa_S-\kappa_{ad}\right)-\frac{l(l+1)}{c_1\omega^2}\right]\right]y_5 \\ &+\frac{V}{\beta}\,\frac{4}{3}\frac{aT^4}{P}\nabla\,y_6 \qquad (A.2) \\ x\frac{\mathrm{d}y_3}{\mathrm{d}x} &= \left(1-U\right)y_3+y_4 \qquad (A.3) \\ x\frac{\mathrm{d}y_4}{\mathrm{d}x} &= U\left(A^*+V_g\right)y_1+U\beta\left(\frac{1}{\Gamma_1}+\upsilon_T\nabla_{ad}\right)y_2+l(l+1)\,y_3 \\ &-U\,y_4+U\left[\frac{4}{3}\frac{aT^4}{P}\left(\frac{1}{\Gamma_1}+\upsilon_T\nabla_{ad}\right)-\upsilon_T\right]y_5 \qquad (A.4) \\ x\frac{\mathrm{d}y_5}{\mathrm{d}x} &= V\,\nabla\left(4-\frac{l(l+1)}{c_1\omega^2}\right)y_1+\beta\left(V\,\nabla\left(\nabla_{ad}\kappa_S-\kappa_{ad}\right)\right. \\ &\left.-\nabla\frac{l(l+1)}{c_1\omega^2}\right)y_2-V\,\nabla\frac{l(l+1)}{c_1\omega^2}\,y_3+\left[V\,\nabla\left(4-\kappa_S\right)\right. \\ &\left.+\frac{4}{3}\frac{aT^4}{P}\left(V\,\nabla\left(\nabla_{ad}\kappa_S-\kappa_{ad}\right)-\nabla\frac{l(l+1)}{c_1\omega^2}\right)\right]y_5 \\ &-V\,\nabla\,y_6 \qquad (A.5) \\ x\frac{\mathrm{d}y_6}{\mathrm{d}x} &= l(l+1)\left(\frac{c_3}{c_1\omega^2}-1\right)y_1 \\ &+\beta\left[c_3\left(\varepsilon_{ad}-\varepsilon_S\nabla_{ad}\right)+\frac{l(l+1)c_3}{c_1\omega^2V}+\mathrm{i}\omega c_4\nabla_{ad}\right]y_2 \\ &-l(l+1)\frac{c_3}{c_1\omega^2}\,y_3+\left[\frac{4}{3}\frac{aT^4}{P}\left(c_3\left(\varepsilon_{ad}-\varepsilon_S\nabla\mathrm{ad}\right)\right.\right. \\ &\left.\left.+\frac{l(l+1)c_3}{c_1\omega^2V}+\mathrm{i}\omega c_4\nabla_{ad}\right)+c_3\varepsilon_S\right. \\ &\left.-\frac{l(l+1)}{\nabla V}-\mathrm{i}\omega c_4\right]y_5-\frac{\mathrm{d}\,\ln L_R}{\mathrm{d}\,\ln r}\,y_6 \qquad (A.6) \end{aligned}$$

where $x = r/R$, and R is the photometric radius. The rest of the variables follow the definitions given in Unno et al. (1989):

$$\begin{aligned} &V_g=\frac{V}{\Gamma_1}=-\frac{1}{\Gamma_1}\frac{\mathrm{d}\ln P}{\mathrm{d}\ln r}=\frac{gr}{c^2} \qquad U=\frac{\mathrm{d}\ln M_r}{\mathrm{d}\ln r}=\frac{4\pi\rho r^3}{M_r} \\ &c=\left(\frac{\Gamma_1 P}{\rho}\right)^{1/2} \qquad c_1=\frac{x^3}{M_r/M} \qquad \omega^2=\frac{\sigma^2R^3}{GM} \qquad (A.7) \end{aligned}$$

$$\begin{aligned} &\beta=\frac{P_g}{P} \quad \nabla_{ad}=\left(\frac{\partial\ln T}{\partial\ln P}\right)_S \quad \nabla=\frac{\mathrm{d}\ln T}{\mathrm{d}\ln P} \quad A^*=\frac{rN^2}{g} \\ &\upsilon_T=-\left(\frac{\partial\ln\rho}{\partial\ln T}\right)_P \quad c_3=\frac{4\pi r^3\rho\varepsilon_N}{L_R} \\ &c_4=\frac{4\pi r^3\rho T c_p}{L_R}\sqrt{\frac{GM}{R^3}} \quad \kappa\,(\text{ or }\varepsilon_N)_{ad}=\left(\frac{\partial\ln\kappa\,(\text{ or }\varepsilon_N)}{\partial\ln P}\right)_S \\ &\kappa\,(\text{ or }\varepsilon_N)_S=c_p\left(\frac{\partial\ln\kappa\,(\text{ or }\varepsilon_N)}{\partial S}\right)_P \qquad (A.8) \end{aligned}$$

N is the Brunt-Väisälä frequency and, M the total mass of the star, κ, is the opacity and, ε_N, is the energy generation rate.

The interior boundary conditions are common to both pulsational treatments, given that the stellar interior is solved using the same equations. In our formalism, these conditions are:

1. The mechanical boundary condition

$$\left(c_1\omega^2-l\right)y_1-\frac{l\beta}{V}\,y_2-l\,y_3-l\frac{4}{3}\frac{aT^4}{PV}\,y_5=0. \qquad (A.9)$$

2. The potential boundary condition

$$l\,y_3-y_4=0. \qquad (A.10)$$

3. The thermodynamical boundary condition

$$-\nabla_{ad}\,\beta\,y_2+\left(1-\frac{4}{3}\frac{aT^4}{P}\nabla_{ad}\right)y_5=0. \qquad (A.11)$$

References

Arentoft, T., Sterken, C., Handler, G., et al. 2001, A&A, 374, 1056
Balona, L. A., & Evers, E. A. 1999, MNRAS, 302, 349
Balona, L. A., & Stobie, R. S. 1979a, MNRAS, 189, 627
Balona, L. A., & Stobie, R. S. 1979b, MNRAS, 189, 649

Breger, M., Pamyatnykh, A. A., Pikall, H., et al. 1999, A&A, 341, 151
Breger, M., Garrido, R., & Handler, G. 2002, MNRAS, 329, 531
Breger, M., Handler, G., Garrido, R., et al. 1999, A&A, 349, 225
Cox, J. P. 1980, Theory of Stellar Pulsation (Princeton: Princeton Univ. Press)
Cugier, H., Dziembowski, W., & Pamyatnykh, A. 1994, A&A, 291, 143
Daszyńska-Daszkiewicz, J., Dziembowski, W. A., Pamyatnykh, A. A., & Goupil, M.-J. 2002, A&A, 392, 151
Daszyńska-Daszkiewicz, J., Dziembowski, W. A., & Pamyatnykh, A. A. 2003, A&A, 407, 999
Dupret, M.-A., De Ridder, J., Neuforge, C., Aerts, C., & Scuflaire, R. 2002, A&A, 385, 563
Dupret, M.-A., De Ridder, J., De Cat, P., et al. 2003, A&A, 398, 677
Dziembowski, W. 1977a, Acta Astron., 27, 95
Dziembowski, W. 1977b, Acta Astron., 27, 203
Garrido, R. 2000, The 6th Vienna Workshop on δ Scuti and related stars, ed. M. Montgommery & M. Breger, PASP Conf. Ser., 210, 67
Garrido, R., Garcia-Lobo, E., & Rodriguez, E. 1990, A&A, 234, 262
Christensen-Dalsgaard, J. 1982, MNRAS, 199, 735
Kurucz, R. L. 1993, ATLAS9 Stellar Atmosphere programs and 2 km s^{-1} grids. Kurucz CDROM No. 13
Morel, P. 1997, A&A, 124, 597
Pesnell, W. D. 1990, ApJ, 363, 227
Saio, H., & Cox, J. P. 1980, ApJ, 236, 549
Townsend, R. 2002, MNRAS, 330, 855
Tran Minh, F., & Leon, L. 1995, Phys. Pross. Ap., 219
Unno, W., Osaki, Y., Ando, H., et al. 1989, Nonradial oscillation of stars (Tokyo: Univ. Tokyo Press)
Watson, R. D. 1988, Ap&SS, 140, 255